Ferrocene-Based Bimetallic MOF Beads as Bifunctional Dye Scavenging and Degrading Materials

Vuyolwethu Tokoyi*, Nirmala Deenadayalu

Durban University of Technology, Faculty of Applied Sciences, P O Box 1334, Durban, South Africa
22290059@dut4life.ac.za

Numerous dye removal techniques have been reported by researchers; however, adsorption and degradation have been identified as the best options due to their low operating costs and greater efficiency. The use of zeolite imidazole based metal organic frameworks (ZIF-MOFs) for dye adsorption and degradation is an effective and preferred approach owing to their desired features such as variable pore diameters and large surface area. Furthermore, there is an increasing interest in using these porous materials to remove toxins from aquatic settings. In this work, two CSM-SA@Ni-MOF composite beads were prepared, evaluated, and used to remove both bromophenol blue (BB, anionic) and malachite green (MG, cationic) dyes from aqueous solutions. Adsorption studies revealed that these materials have good anionic and cationic dye capture ability which is primarily due to the electrostatic interaction between the materials' surface positive or negative charges, as well as the affinity of the interlinked natural adsorbents (chitosan and sodium alginate) for the dyes, and excellent reusability.
Keywords: Malachite green (MG), bromophenol blue (BB), ZIF-MOFs, CSM-SA@Ni-MOF beads

1. Introduction

Dye toxicity and nonbiodegradability have emerged as global issues, posing a serious threat to the environment, particularly in water (Kaur et al. 2023). Safe drinking water is necessary for healthy living, but water pollution by organic and inorganic toxins has a severe influence on both human health and the ecosystem (Zadehahmadi et al. 2023). These pollutants are most typically found in industrial effluent (Pouramini et al. 2023), hospital, and agricultural wastewater discharge (Abdi and Abedini 2020). Numerous strategies for dye removal in aqueous solutions have been investigated to far, but the most effective and favoured strategy is adsorption and degradation utilizing ZIF-MOFs (Zadehahmadi et al. 2023).

Zeolite imidazole metal-organic frameworks (ZIF-MOFs) are porous crystalline materials with good qualities that allow them to be used as gas capturers (Ortiz-Albo et al. 2022), dye adsorbents (Patel et al. 2021), catalysts (Babu et al. 2023), heavy metal adsorbers (Li et al. 2021), and so on (Hou et al. 2019). They have been demonstrated to be effective in all these applications but still, in other cases, they are difficult to separate, thus preparing them as beads has shown to be more practical, easier to handle (Zhao et al. 2023), and separate from the mixture (Liu et al. 2019). The most frequent materials utilized to successfully manufacture these beads are natural polymers, synthetic polymers, or a mix of the two. CSM-SA hybrid beads were previously investigated for heavy metal removal in aqueous solutions and proven to be excellent green adsorbents for lead (II) and chromium (VI) heavy metals (Aljar, Rashdan and Abd El-Fattah 2021).

In this study, Ni-MOFs were combined with chitosan and sodium alginate polymers to create flexible hybrid MOF-based beads that were utilized to segregate and degrade dyes in water, with potent industrial application for textile wastewater (TWW) treatment (Aljar, Rashdan and Abd El-Fattah 2021). The Ni-MOFs were synthesized and characterized using Fourier Transform Infrared Spectroscopy (Agilent Cary 360 FTIR, DUT), Ultra-violet visible spectroscopy (Thermo Scientific GENESYS 40/50 UV-Vis), scanning electron microscopy (SEM) and SEM-EDX analysis. CSM-SA, CSM-SA@Ni:NTAA, and CSM-SA@Ni+Fe:NTAA beads were prepared and evaluated for dye adsorption and degradation in aqueous solutions. The preparation and adsorption procedures are included as supplementary data.

2. Results and discussion

2.1 Characterization of MOFs

Superimposed electronic spectra obtained from UV-Vis of the MOFs illustrated π→π* and n→π* in a range of 280-300 nm attributed to N−C and C−O−O bonds, and d-d transitions at 675 nm (Ni:NTAA), 322, 440, and 728 nm (Ni+Fe:NTAA). The functional groups of MOFs were analyzed and obtained over a range 4000−650 cm^{-1}, illustrated stretching frequencies at 3395-3283 cm^{-1}, 2460 cm^{-1}, 1405 cm^{-1}, 2817 cm^{-1}, and 1681-1699 cm^{-1}, associated with v(O−H), v(N−C), v(C−O), v(C−H) (sp^3), and v(C=O) stretching vibrations (Figure S2). The surface morphology of each MOF illustrated a porous and rough surface with an intertwined polymer network demonstrating a successful impartment of the compounds (Figure S3). EDX elemental mapping confirmed the presence of Fe(II), Ni(II), O, S, C, and N (Figure S4).

2.2 Swelling behavior of CSM-SA@Ni-MOF beads

Water absorption of chitosan (CSM) alone decreases with increasing pH, while that of sodium alginate (SA) rises with pH. This is due to the de-ionization of the carboxyl groups, which results in either an increase (with pH increase) or a decrease (with pH drop) in electrostatic repulsive force (Liu *et al.* 2019). The -OH groups attract water molecules into the polymer network, resulting in varying swelling percentages based on the size and accessible pores (Aljar, Rashdan and Abd El-Fattah 2021). Combining the features of both polymers yielded CSM-SA crosslinked polymer-based beads with good swelling capabilities, as seen in Figure 2a. The acquired average swelling values of the beads in deionized water about change in pH all demonstrated a similar trend: as pH increases, so do the average swelling percentages. This discovery is attributable to the crosslinked structure of CS and SA (as shown in Figure 2b), which provides better adsorption and swelling capabilities via ionic interactions between the NH_3^+ CS groups and the OH and COO- groups of SA (Ablouh *et al.* 2019).
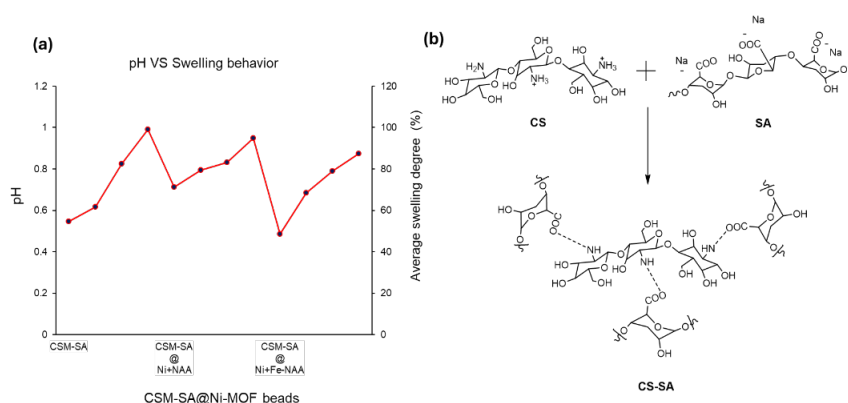

Figure 2: (a) Effect of pH on the beads swelling behavior and (b) cross-linked CS and SA polymer network.

Figure 2a at pH=3, CSM@SA beads swelling percentage is 54.66 %, CSM-SA@Ni:NTAA and CSM-SA@Ni+Fe:NTAA percentage values are 71.24 % and 48.67 % respectively. This enhanced swelling to the ZIF-MOF-based beads is attributed to the MOF porous material that can trap water molecules and are also known as good adsorbents. This trend is observed only until pH=7, at pH=9, the pristine beads have a swelling percentage value of 99.13 %, while for CSM-SA@Ni:NTAA and CSM-SA@Ni+Fe:NTAA the values are 94.8 % and 87.34 % respectively. This reduction in swelling in an alkaline pH is due to the structural change within the polymer matrix after incorporating the MOF porous materials (Abdi and Abedini 2020; Zeng *et al.* 2022; Zhao *et al.* 2023). Even though it has been noted for pristine beads to have a good swelling property, creating more space to be occupied by the water molecules, resulting in more water uptake and a higher degree of swelling among the examined beads, CSM-SA@Ni:NTAA and CSM-SA@Ni+Fe:NTAA bead expansion is restricted because these porous materials are within the polymer matrix and do not swell or dissolve when in contact with aqueous solutions, and it was expected.

3. Adsorption studies

Adsorption kinetics

The adsorption kinetics of CSM@SA, CSM-SA@Ni:NTAA, and CSM-SA@Ni+Fe:NTAA beads at various contact times were investigated. These investigations are critical for determining the efficiency and pace of

adsorption to equilibrium. The kinetics and adsorption efficiency (AE) of MG and BB on the compounds were investigated using two kinetic models, pseudo-first-order (PFO, linearized and non-linear) and pseudo-second-order (PSO, linearized and non-linear), which are given as Equations 4 (Aljar, Rashdan and Abd El-Fattah 2021), 5 (Karami *et al.* 2022) and 6 (Abdi and Abedini 2020).

$$\ln(q_e - q_t) = \ln q_e - K_1 t \tag{4}$$

$$\tag{5}$$

$$q_t = \frac{K_2 q e^2 t}{1 + K_2 q_e t}$$

$$AE\% = \frac{C_i - C_e}{C_i} \, x100 \tag{6}$$

q_e and q_t (mg/g) refer to dye adsorption capacity at t (min), and K (g/mmol/min) is the kinetic rate constant. The determined kinetic model parameters and their corresponding R^2 values are summarized in Table S5 and S6. Figure 3 illustrates the adsorption efficiency (AE) percentage values at 15-minute interval sampling for both MG and BB dyes increases. At 150 minutes, pristine CSM@SA beads have an AE of 78.60 %, CSM-SA@Ni:NTAA and CSM-SA@Ni+Fe:NTAA beads have AE values of 82.0 % and 87.50 % in MG dye solutions, while in BB dye solutions,   CSM@SA, CSM-SA@Ni:NTAA and CSM-SA@Ni+Fe:NTAA beads, have AE values of 66.7 %, 86.0 % and 90.80% respectively. The enhanced adsorption efficiency values obtained for CSM-SA@Ni:NTAA and CSM-SA@Ni+Fe:NTAA materials in both MG and BB dye solutions when compared to the pristine beads is associated with the incorporated MOF materials (which are commonly known as good adsorbents (Patel *et al.* 2021) within the polymer network.
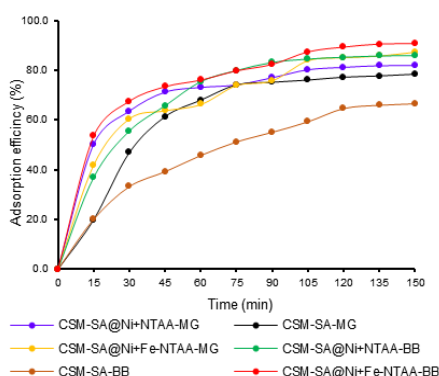

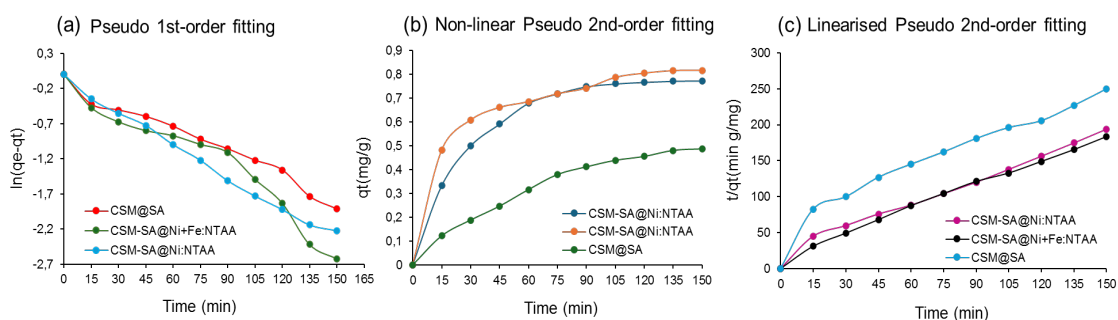*Figure 3: Removal percentage efficiency of both MG and BB dye solutions*

Figure 4: Kinetic adsorption for BB using (a) Pseudo 1st order fitting, (b) Non-linear pseudo 2nd order (c) Linearized pseudo 2nd order fitting models

Figure 4 shows BB adsorption kinetics, where (a) adsorption curves for CSM-SA and CSM-SA@Ni:NTAA beads were better expressed using a pseudo-first-order model, with the values of the correlation coefficient (R_1^2) being higher than those obtained from pseudo-second-order (Table S6), and suggesting a physisorption mechanism, while in Figure 4b, CSM-SA@Ni+Fe:NTAA adsorption curve is better expressed using pseudo-second-order (non-linear), suggesting a chemisorption mechanism (Abdi and Abedini 2020; Zeng *et al.* 2022; Zhao *et al.* 2023).

Figure 5 shows MG adsorption kinetics, where (b) adsorption curves for CSM@SA, CSM-SA@Ni:NTAA and CSM-SA@Ni+Fe:NTAA beads were better expressed using a pseudo-second-order model, with the values of the correlation coefficient (R_2^2) being higher than those obtained from pseudo-first-order (Table S7). This model suggests a chemisorption property during MG dye adsorption kinetics (Abdi and Abedini 2020; Zeng *et al.* 2022; Zhao *et al.* 2023).
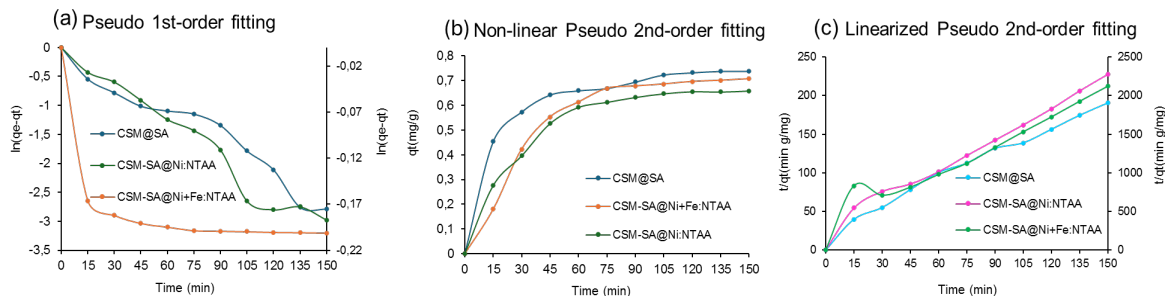

Figure 5: Kinetic adsorption for MG using (a) Pseudo 1st order fitting, (b) Non-linear pseudo 2nd order (c) Linearized pseudo 2nd order fitting models.

Adsorption isotherms

The interaction between dyes and CSM@SA, and CSM-SA@Ni-MOF beads was studied using the Langmuir and Freundlich models to get a better knowledge of the adsorption process and maximum adsorption capacity of the adsorbents (Zhao *et al.* 2023). The resulting experimental data was quantitatively analyzed using Equations 6 to 8 below reported by Karami *et al.* (2022).

$$q_e = \frac{q_m K_L C_e}{1 + K_L C_e} \tag{6}$$

$$R_L = \frac{1}{1 + K_L C_0} \tag{7}$$

Where q_m (mg/g) is the maximum monolayer adsorption capacity, q_e (mg/g) is the amount of the adsorbed dye at equilibrium, C_e (mg/L) is the equilibrium concentration, K_L is the Langmuir constant associated with adsorption rate and affinity of the binding sites. R_L (separation factor) reflects the nature of the Langmuir model (Fan *et al.* 2018) where if the value is between 0 and 1, the process if favorable (Karami *et al.* 2022).

$$q_e = K_f C_e^{\,1/n} \tag{8}$$

Where n and K_f ($mg^{1-1/n}\,L^{-1/n}\,g^{-1}$) are Freundlich constants that represent adsorption capacity and intensity respectively, and if $1/n$ value is between 0 and 1, then the adsorption process is a multilayered adsorption and favorable (Fan *et al.* 2018; Karami *et al.* 2022). Figure 6 (a) to (f) displays the isotherm equilibrium distribution of the experimental data obtained from using CSM-SA, CSM-SA@Ni:NTAA and CSM-SA@Ni+Fe:NTAA adsorbents in both BB and MG dye solutions at different initial concentrations, to accurately follow both non-linear fitting isotherm models when compared to the linearized models, and with very high R^2 values depicted in Table S8 (BB dye solutions) and S9 (MG dye solutions). This indicates the suitability of both models and the description of the adsorption mechanism of both dyes on the adsorbents to both have monolayer adsorption on homogenous surfaces and multilayer adsorption on heterogeneous surfaces (Aljar, Rashdan and Abd El-Fattah 2021).

The Langmuir dimensionless separation factor (R_L) was determined using the Langmuir constant value K_L (mg/L) to determine the separation performance of CSM-SA@Ni:NTAA, CSM-SA@Ni+Fe:NTAA, and CSM-SA beads. Figure S9 depicts the R_L used to explain the adsorption experimental data of both MG and BB dyes across three adsorbents. The R_L values of CSM-SA for both BB and MG adsorptions are 0.4098-0.9960 (Table S8 and S9), and for CSM-SA@Ni:NTAA and CSM-SA@Ni+Fe:NTAA, the values are 0.5348-0.9926 and 0.2410-0.9661 (Table S3 and S4), respectively. The $0 < R_L < 1$ implies favorable Langmuir adsorption isotherms for both BB and MG dyes on adsorbents [10]. Notably, the RL value decreases as concentration increases, which is related to the influence of pH_{pzc} of each adsorbent on each dye, as well as how concentration affects maximum adsorption capacity.

The favourability of the Freundlich adsorption isotherms was determined, and the resultant Freundlich constant values (1/n) for both MG and BB dye were within the range of 0.74-1.47 (Table S8 and S9), respectively. CSM-

SA has 1/n = 0.74 (MG), and 1.33 (BB). This indicates that the MG dye adsorption was more favorable than BB dye adsorption process, while for CSM-SA@Ni:NTAA and CSM-SA@Ni+Fe:NTAA, 1/n = 0.99 (MG) and 0.92 (BB), and 1.43 (MG) and 1.47 (BB). These obtained values indicate that both adsorption processes for MG and BB dye in CSM-SA@Ni:NTAA were more favorable than those of CSM-SA@Ni+Fe:NTAA. This effect is a result of less pores available for adsorption in the ferrocene-based material than in the Ni-based material (Fan *et al.* 2018; Karami *et al.* 2022).
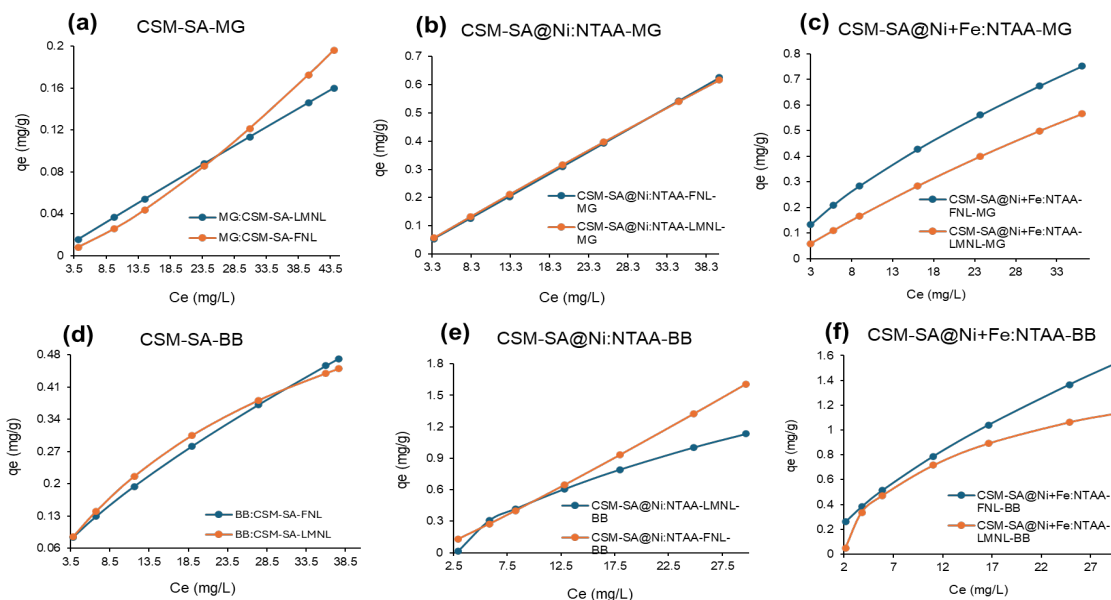

Figure 6: Langmuir and Freundlich adsorption isotherms for MG and BB dye solutions (LMNL- Langmuir non-linear and FNL- Freundlich non-linear)

4. Photocatalytic dye degradation

MG and BB were both tested for degradation under UV light irradiation in the presence of CSM-SA@Ni:NTAA and CSM-SA@Ni+Fe:NTAA beads. Figure 7(a and b) shows that the photocatalytic activity of CSM-SA@Ni+Fe:NTAA beads degraded both MG and BB significantly over time when compared to CSM-SA@Ni:NTAA beads.
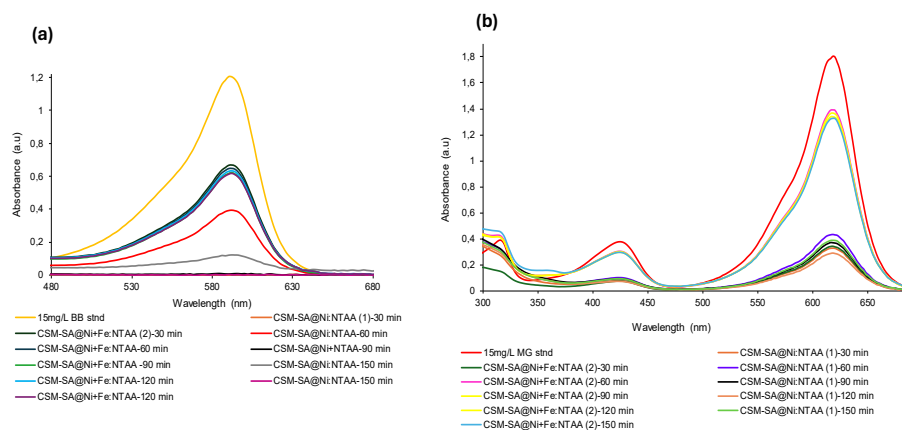

Figure 7: Langmuir separation performance evaluation of CSM-SA@Ni-MOF beads in MB and BB dye solutions

5. Conclusions

Coupling ZIF-MOFs with flexible natural polymers (chitosan and sodium alginate) provided a quick, simple, and convenient way to produce flexible MOF materials that are efficient in absorbing and degrading organic dyes. CSM-SA@Ni:NTAA and CSM-SA@Ni+Fe:NTAA adsorbents were prepared by crosslinking CSM with SA, and

incorporating the Ni-MOFs. The embedded MOF materials not only enhanced the adsorption effect but also showed remarkably higher photocatalytic dye degradation activity, especially when coupled with ferrocene. These hybrid beads as adsorbents have the potential to also be further investigated at a pilot scale (filtration system), then industrially for organic dye removal in a variety of industries, like textile.

Acknowledgments

References

Abdi, J. and Abedini, H. 2020. MOF-based polymeric nanocomposite beads as an efficient adsorbent for wastewater treatment in batch and continuous systems: Modelling and experiment. *Chemical Engineering Journal*, 400: 1-13.

Ablouh, E., Hanani, Z., Eladlani, N., Rhazi, M. and Taourirte, M. 2019. Chitosan microspheres/sodium alginate hybrid beads: an efficient green adsorbent for heavy metals removal from aqueous solutions. *Sustainable Environment Research*, 29 (1): 1-11.

Aljar, M. A. A., Rashdan, S. and Abd El-Fattah, A. 2021. environmentally friendly polyvinyl alcohol-alginate/bentonite semi-interpenetrating polymer network nanocomposite hydrogel beads as an efficient adsorbent for the removal of methylene blue from aqueous solution. *Polymers (Basel)*, 13 (22): 1-19.

Babu, S., Jojo, L., James, A., Melethil, K. and Thomas, B. 2023. Metal-based catalysis for biomass and renewables valorization- current status. *Tetrahedron Green Chem*, 2: 1-17.

Fan, C., Liang, Y., Dong, H., Yang, J., Tang, G., Zhang, W., Kong, D., Li, J. and Cao, Y. 2018. Guanidinium ionic liquid-controlled synthesis of zeolitic imidazolate framework for improving its adsorption property. *Science of the Total Environment,* 641: 163-173.

Hou, J., Hao, J., Wang, Y. and Liu, J. 2019. Synthesis of CuII/ZIF-8 Metal-organic framework catalyst and its application in the aerobic oxidation of alcohols. *Chemical Research in Chinese Universities*, 35 (5): 860-865.

Karami, A., Shomal, R., Sabouni, R., Al-Sayah, M. H. and Aidan, A. 2022. Parametric study of methyl orange removal using metal–organic frameworks based on factorial experimental design analysis. *Energies*, 15 (13): 1-23.

Kaur, H., Devi, N., Siwal, S. S., Alsanie, W. F., Thakur, M. K. and Thakur, V. K. 2023. Metal-organic framework-based materials for wastewater treatment: superior adsorbent materials for the removal of hazardous pollutants. *ACS Omega*, 8 (10): 9004-9030.

Li, K., Miwornunyuie, N., Chen, L., Jingyu, H., Amaniampong, P. S., Ato Koomson, D., Ewusi-Mensah, D., Xue, W., Li, G. and Lu, H. 2021. Sustainable Application of ZIF-8 for heavy-metal removal in aqueous solutions. *Sustainability*, 13 (2): 1-11.

Liu, L., Yang, W., Gu, D., Zhao, X. and Pan, Q. 2019. In situ preparation of chitosan/ZIF-8 composite beads for highly efficient removal of U(VI). *Frontiers in Chemistry*, 7: 1-10.

Ortiz-Albo, P., Ferreira, T. J., Martins, C. F., Alves, V., Esteves, I. A. A. C., Cunha-Silva, L., Kumakiri, I., Crespo, J. and Neves, L. A. 2022. Impact of ionic liquid structure and loading on gas sorption and permeation for Zif-8-based composites and mixed matrix membranes. *Membranes,* 12: 1-32.

Patel, U., Parmar, B., Dadhania, A. and Suresh, E. 2021. Zn(II)/Cd(II)-based metal-organic frameworks as bifunctional materials for dye scavenging and catalysis of fructose/glucose to 5-hydroxymethylfurfural. *Inorganic Chemistry*, 60 (12): 9181-9191.

Pouramini, Z., Mousavi, S. M., Babapoor, A., Hashemi, S. A., Lai, C. W., Mazaheri, Y. and Chiang, W.-H. 2023. Effect of metal atom in zeolitic imidazolate frameworks (ZIF-8 & 67) for removal of dyes and antibiotics from wastewater: a review. *Catalysts*, 13 (1): 1-30.

Zadehahmadi, F., Eden, N. T., Mahdavi, H., Konstas, K., Mardel, J. I., Shaibani, M., Banerjee, P. C. and Hill, M. R. 2023. Removal of metals from water using MOF-based composite adsorbents. *Environmental Science: Water Research & Technology*, 9 (5): 1305-1330.

Zeng, H., Sun, S., Xu, K., Zhao, W., Hao, R., Zhang, J. and Li, D. 2022. Adsorption of As(V) by magnetic alginate-chitosan porous beads based on iron sludge. *Journal of Cleaner Production*, 359: 1-12.

Zhao, Y., Yuan, N., Bian, D., Sun, J. and Qian, G. 2023. Preparation of a novel CSM@ZIF-67 composite microsphere to facilitate congo red adsorption from dyeing wastewater. *Environmental Technology*: 1-13.